scientific reports

Check for updates

OPEN

Voxel-S-Value based 3D treatment planning methods for Y-90 microspheres radioembolization based on Tc-99m-macroaggregated albumin SPECT/CT

Gefei Chen[1], Zhonglin Lu[1], Han Jiang[1], Ko-Han Lin[3] & Greta S. P. Mok[1,2]✉

Partition model (PM) for Y-90 microsphere radioembolization is limited in providing 3D dosimetrics. Voxel-S-Values (VSV) method has good agreement with Monte Carlo (MC) simulations for 3D absorbed dose conversion. We propose a new VSV method and compare its performance along with PM, MC and other VSV methods for Y-90 RE treatment planning based on Tc-99m MAA SPECT/CT. Twenty Tc-99m-MAA SPECT/CT patient data are retrospectively analyzed. Seven VSV methods are implemented: (1) local energy deposition; (2) liver kernel; (3) liver kernel and lung kernel; (4) liver kernel with density correction (LiKD); (5) liver kernel with center voxel scaling (LiCK); (6) liver kernel and lung kernel with density correction (LiLuKD); (7) proposed liver kernel with center voxel scaling and lung kernel with density correction (LiCKLuKD). Mean absorbed dose and maximum injected activity (MIA) obtained by PM and VSV are evaluated against MC results, and 3D dosimetrics generated by VSV are compared with MC. LiKD, LiCK, LiLuKD and LiCKLuKD have the smallest deviation in normal liver and tumors. LiLuKD and LiCKLuKD have the best performance in lungs. MIAs are similar by all methods. LiCKLuKD could provide MIA consistent with PM, and precise 3D dosimetrics for Y-90 RE treatment planning.

Abbreviations

CECT	Contrast enhanced CT
CI	Confidence interval
DVH	Dose-volume histogram
EBRT	External beam radiation therapy
IA	Injected activity
LED	Local energy deposition
LDCT	Low-dose CT
LiCK	Liver kernel with center voxel scaling
LiCKLuKD	Liver kernel with center voxel scaling and lung kernel with density correction
LiK	Liver kernel
LiKD	Liver kernel with density correction
LiLuK	Liver kernel and lung kernel
LiLuKD	Liver kernel and lung kernel with density correction
LSF	Lung shunt fraction
MAA	Macroaggregated albumin
MC	Monte Carlo
MIA	Maximum injected activity
NL	Nontumoral liver
RE	Radioembolization
TNR	Tumor to normal liver ratio

[1]Biomedical Imaging Laboratory (BIG), Department of Electrical and Computer Engineering, Faculty of Science and Technology, University of Macau, Avenida da Universidade, Taipa, Macau SAR, China. [2]Ministry of Education Frontiers Science Center for Precision Oncology, University of Macau, Macau, SAR, China. [3]Department of Nuclear Medicine, Taipei Veterans General Hospital, Taipei, Taiwan. ✉email: gretamok@um.edu.mo

VOI   Volume-of-interest
VSV   Voxel-S-Value

Y-90 microspheres radioembolization (RE) is an effective treatment for patients with primary and metastatic liver cancers[1]. Microspheres labeled with Y-90 are delivered to tumors through the hepatic artery and then trapped preferentially in tumoral tissue capillaries. Radiation dose delivered to tumors should be high enough to ensure therapeutic efficacy[2], which inevitably leads to radiation to the surrounding normal tissues, possibly causing nontumoral liver (NL) complications[3] and radiation pneumonitis[4]. Thus, to ensure both internal radiation protection and treatment efficacy, treatment planning based on pre-treatment quantitative imaging is essential to realize personalized Y-90 RE for patients[5].

Body surface area method and partition model are recommended for injected activity (IA) calculation of resin microspheres[6,7], while standard model and partition model are suggested for IA calculation of glass microspheres[8]. The calculation of IA by body surface area method depends on the volume of tumors and NL, and patient's height and weight. Standard model concerns radiation dose of two compartments, i.e., liver and lungs[9]. Partition model divides the radiation-affected volume into three compartments, i.e., NL, tumors and lungs[10]. All methods require pre-treatment Tc-99m-macroaggregated albumin (MAA) planar or SPECT/CT scans to estimate the distribution of microspheres after RE. Lung shunt fraction (LSF) and tumors to normal liver ratio (TNR) should be determined from Tc-99m-MAA images and the maximum injected activity (MIA) can then be calculated based on the preset absorbed dose limits for NL and lungs for partition model. Although the three aforementioned treatment planning methods partially implement the individualized dose calculation, they only consider the mean absorbed dose and assume a uniform activity distribution throughout the compartments. On the other hand, the dose-volume histogram (DVH), calculated from voxel-level absorbed dose map, could describe the heterogeneous absorbed dose distribution within a volume-of-interest (VOI). It is frequently used in the external beam radiation therapy (EBRT) for treatment planning, and has been shown as a valuable tool for the evaluation of tumor control probability[11] and normal tissue toxicity[12] in Y-90 RE.

Voxel-S-Value (VSV) method is used to calculate the voxel-level absorbed dose for heterogeneous activity in a uniform medium[13], serving as an efficient alternate to the gold standard yet time consuming Monte Carlo (MC) approach. Moreover, local energy deposition (LED), a special case of VSV, is commonly used for Y-90 absorbed dose conversion as it is a pure β^- emitter with shorter travelling range[14]. Several improved VSV methods for heterogeneous medium have been investigated, e.g., density correction[15], tissue-specific VSV[16] and center voxel scaling[17]. However, they are still compromised in absorbed dose estimation of liver-lungs interface[18]. Meanwhile, recent studies have presented 3D dosimetry treatment planning methods based on Tc-99m-MAA SPECT/CT for Y-90 RE, showing superior dosimetric results to partition model by taking inhomogeneous microspheres distributions into consideration[19–21]. These studies are based on MC, LED and standard VSV methods. Besides, the accuracy of DVH in targeted VOIs obtained by VSV methods has not been well evaluated.

In this work, we evaluated the performance of seven VSV methods, including a newly proposed tissue-specific VSV method with density correction, i.e., liver kernel with center voxel scaling and lung kernel with density correction (LiCKLuKD)[22], on 3D dosimetrics calculations using Tc-99m-MAA SPECT/CT. Standard partition model and MC results were also compared.

Materials and methods

Imaging protocol and data preprocessing. Twenty sets of Tc-99m-MAA SPECT/CT patient data from University of Michigan Deep Blue Data sharing repository (n = 6)[23] and Taipei Veterans General Hospital (n = 14) were analyzed in this study. The detailed imaging protocol for the Deep Blue Data was described in a related literature[24]. The tumor maps were available in the Deep Blue dataset, while the liver and lung maps were segmented from CT images. All images and maps were down-sampled to match with the original voxel size of SPECT images ($4.8 \times 4.8 \times 4.8$ mm³) for further dose calculation and analysis.

Fourteen sets of patient data from Taipei Veterans General Hospital with malignant liver tumors, who underwent both contrast enhanced CT (CECT) (MIYABI angio-CT, Siemens Healthineers, Germany) and Tc-99m-MAA SPECT/CT (Discovery NM670, GE Healthcare, USA) were retrospectively analyzed. All procedures performed in this study were approved by the Institutional Review Board of Taipei Veterans General Hospital, in accordance with the 1964 Helsinki declaration and its later amendments or comparable ethical standards. Institutional Review Board of Taipei Veterans General Hospital waived the requirement of informed consent due to the retrospective nature of this study without patient-identifiable information. All patients were administered with 111 MBq Tc-99m-MAA to simulate the Y-90 microspheres distribution for treatment planning. CECTs were collected for segmentation of tumors with a voxel size of $0.68 \times 0.68 \times 5.00$ mm³ and a matrix size of $512 \times 512 \times 44$, covering the whole liver and partial bottom lungs. Sixty SPECT projections covering the whole liver and whole lungs were acquired with a low-energy high-resolution collimator over 360°, with a primary window of 126–154 keV and a scatter window of 114–126 keV. These projections were then reconstructed with ordered subset expectation maximization (2 iterations, 10 subsets), incorporating CT-based attenuation correction and dual-energy window-based scatter correction. The SPECT reconstruction voxel size is $4.42 \times 4.42 \times 4.42$ mm³ and the matrix size is $128 \times 128 \times 128$. Corresponding low-dose CT (LDCT) data covering whole liver and whole lungs were acquired (120 kV, 57 mA) during shallow free breathing, with a reconstructed voxel size of $0.98 \times 0.98 \times 3.75$ mm³ and a matrix size of $512 \times 512 \times 108$.

The tumor map was segmented in CECT by an experienced radiologist due to its distinct tumor contours. CECT and tumor map were aligned to LDCT by rigid registration using Elastix[25]. Then, VOIs of whole liver and whole lungs were manually delineated in LDCT. The NL contours were obtained by excluding the tumors from

the whole liver. Finally, LDCT and VOI maps, i.e., liver, lungs and tumors, were downsampled to match with the voxel size of SPECT images for further dose calculation and analysis.

SPECT/CT fusion images, CECT and VOI binary maps of two sample patients were shown in Fig. 1. SPECT and corresponding CT images were all well aligned in this study. LDCT images were converted to density maps and tissue maps for MC- and VSV-based absorbed dose conversion[26]. Activity in each voxel (A) was obtained through a self-calibration factor defined as the (total injected activity)/(counts in the SPECT images covering whole liver and lungs)[27]. The time-integrated activity (TIA) images $\tilde{A}$ were generated assuming the microspheres were all trapped in tumors with only physical decay afterwards:

$$\tilde{A}_{Voxel} = \frac{A_{Voxel}}{\lambda} \tag{1}$$

where $\lambda = \ln 2 / T_{1/2}$, $T_{1/2} = 64.04$ h for Y-90.

MC simulation and VSV generation.

MC simulation and VSV generation were performed using GATE v.9.0, which has been validated in Y-90 dosimetry previously[28]. Y-90 emitter was simulated by defining an ion source. The physics list emstandard_opt4 was used in the simulation, including photoelectric effect, Compton scattering, Rayleigh scattering, multiple scattering and pair production modeled for photons, while positron annihilation, ionization and bremsstrahlung effect were modeled for β particles. Cutting energy of 10 keV was set for all particles to reduce the simulation time. Density map and tissue map were input for creating the voxelized phantom, and TIA images were read in as the voxelized source. A total number of 10^{10} primary decays were simulated. The statistical uncertainty of mean absorbed dose by MC simulation is 0.02% for liver and 0.78% for lungs. DoseActor was attached to the voxelized phantom to collect the 3D absorbed dose distribution. VSVs for lungs ($\rho_{Lung} = 0.26$ g/cm^3) and liver ($\rho_{Liver} = 1.06$ g/cm^3) were also generated using GATE, with the same voxel size as the two sets of SPECT images used in this study and a matrix size of $21 \times 21 \times 21$ and $5 \times 5 \times 5$ respectively, to include > 99% released energy. A total of 10^9 primaries were set for all VSV simulations to ensure uncertainties < 0.01%. To speed up the simulation, all simulations were split into 64 subsets with different random seeds for parallel running in the cluster with four Xeon 6248 CPUs and 128 GB RAM.

VSV-based absorbed dose conversion.

Local energy deposition (LED) method requires the mean energy of β particles and the mass of each voxel for voxel-level dose calculations, serving as a special case of VSV in this study:

$$D_{Voxel} = \tilde{A}_{Voxel} \times \frac{E}{M} \tag{2}$$

where D_{Voxel} is the voxel dose of a 3D absorbed dose map, is the multiplication operator, E is the mean energy of Y-90, i.e., 49.67 (J/GBq), and M is the mass of a voxel.

Other six VSV methods are evaluated in this study:

1. Liver kernel (LiK)[13]:
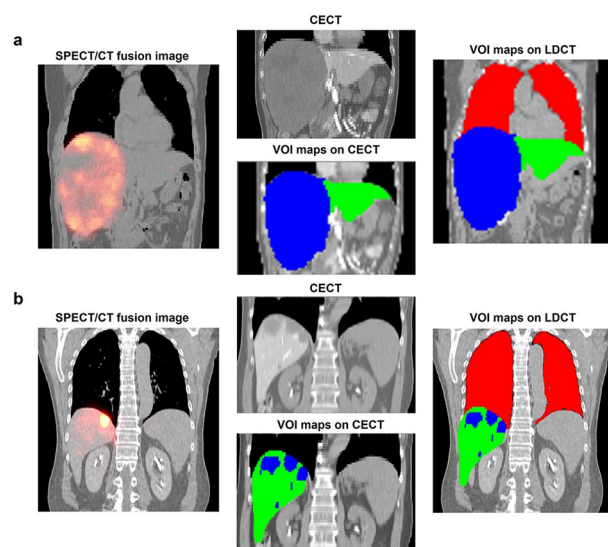
Figure 1. Two sample patients with (**a**) a single tumor and (**b**) multiple tumors. Red: lungs, blue: tumors, green: NL.

$$D = \tilde{A} \otimes K_{Liver} \tag{3}$$

where is the convolution operator, $\tilde{A}$ is the whole body TIA map and K_{Liver} is the liver VSV.

2. Liver kernel for liver TIA and lung kernel for lung TIA (LiLuK)[16]

$$D = \tilde{A}_{Liver} \otimes K_{Liver} + \tilde{A}_{Lungs} \otimes K_{Lung} \tag{4}$$

where $\tilde{A}_{Liver}$ is the liver TIA map, $\tilde{A}_{Lung}$ is the lung TIA map and K_{Lung} is the lung VSV.

3. Liver kernel with density correction (LiKD)[15]

$$D = \tilde{A} \otimes K_{Liver}^{D} \tag{5}$$

where $K_{Liver}^{D}(i,j,k) = K_{Liver}(i,j,k)\frac{\rho_{Liver}}{\rho(i,j,k)}$, $\rho(i,j,k)$ indicates the density of voxel (i, j, k).

4. Liver kernel with center voxel scaling (LiCK)[17]

$$D = \tilde{A} \otimes K_{Liver}^{C} \tag{6}$$

where $K_{Liver}^{C} = K_{Liver}\frac{\rho_{Liver}}{\rho_{centervoxel}}$ and $\rho_{centervoxel}$ means the voxel density corresponding to the voxel where the VSV center locates during the convolution.

5. Liver kernel and lung kernel with density correction (LiLuKD)[29]

$$D = \tilde{A}_{Liver} \otimes K_{Liver}^{D} + \tilde{A}_{Lungs} \otimes K_{Lung}^{D} K \tag{7}$$

where $K_{Lung}^{D}(i,j,k) = K_{Lung}(i,j,k)\frac{\rho_{Lung}}{\rho(i,j,k)}$.

6. Newly proposed LiCKLuKD

$$D = \tilde{A}_{Liver} \otimes K_{Liver}^{C} + \tilde{A}_{Lungs} \otimes K_{Lung}^{D} \tag{8}$$

Dosimetry assessment. The accuracy of D_{NL}^{mean}, D_{Tumors}^{mean} and D_{Lungs}^{mean} obtained by partition model and VSV methods were evaluated against MC results. The DVH dosimetrics of NL, tumors, and lungs generated by VSV methods were also evaluated with MC results. All dosimetric calculations were based on an IA of 3 GBq, which is the MIA suggested by the empirical method[30] and semi-empirical body surface area method[31]. Other dosimetrics commonly used in EBRT[32] were also evaluated for VSV methods and compared with MC results: percentage of the volumes receiving at least 70 Gy for NL ($V_{NL, 70 Gy}$), 200 Gy for tumors ($V_{Tumors, 200 Gy}$), 5 Gy ($V_{Lungs, 5 Gy}$) and 13 Gy ($V_{Lungs, 13 Gy}$) for lungs.

To evaluate the DVH accuracy, the mean absolute error (MAE) of the differential DVH in each VOI was calculated for VSV methods as compared to MC according to Eq. 9[33], based on absorbed dose bins of 1 Gy:

$$MAE = \frac{1}{\text{maximum absorbed dose}} \sum_{k=1}^{\text{maximum absorbed dose}} |V_{VOI,k}^{VSV} - V_{VOI,k}^{MC})| \tag{9}$$

where k is the absorbed dose bin index, and VOI includes tumors, NL and lungs. Cumulative DVH is also generated for the sample patients.

Injected activity assessment. Assuming that Y-90 microspheres and Tc-99m-MAA have the same distribution, MIA is determined by considering the upper absorbed dose limit of lung and NL absorbed dose. For partition model, the LSF and TNR values need to be measured from Tc-99m-MAA planar or SPECT images.

$$LSF(\%) = 100\% \times \frac{A_{Lungs}}{A_{Lung} + A_{Liver}} \tag{10}$$

where A_{Lungs} is the activities of the lungs and A_{Liver} is the activities of the whole liver.

$$TNR = \frac{A_{Tumors}/M_{Tumors}}{A_{NL}/M_{NL}} \tag{11}$$

where A_{Tumors}, A_{NL} and M_{Tumors}, M_{NL} are the activities and mass of tumors and NL, respectively. Mass for partition model is calculated based on the volumes measured from CT and assuming a uniform density of liver (1.06 g/cm³) and lungs (0.26 g/cm³).

MIA can be calculated from the following equation:

$$MIA_{PM} = \min\left[\frac{(M_{Tumors} \times TNR + M_{NL}) \times D_{NL}^{max}}{49.67 \times (1 - LSF/100)}, \frac{M_{Lungs} \times D_{Lungs}^{max}}{49.67 \times LSF/100}\right] \tag{12}$$

where D_{NL}^{max} and D_{Lungs}^{max} is the upper limit of NL and lungs absorbed dose respectively, and usually set to 70 Gy and 30 Gy in partition model, while 49.67 (J/GBq) is the constant converting TIA to absorbed dose.

The MIA for the 3D dosimetric models is obtained as follows:

$$MIA_{3D} = \min\left[\frac{D_{NL}^{max}}{D_{NL}^{mean}/IA_{MAA}}, \frac{D_{Lungs}^{max}}{D_{Lungs}^{mean}/IA_{MAA}}\right] \quad (13)$$

D_{NL}^{max} is 70 Gy and D_{Lungs}^{max} is 30 Gy. D_{VOI}^{mean} is the mean absorbed dose calculated by MC and VSV. and IA_{MAA} is 111 MBq for data from Taiwan and 222 MBq for Deepblue data. MIA calculated by partition model and VSV methods were compared with MC results.

The two-tailed paired samples Wilcoxon test with Bonferroni correction was performed between results of MC and other methods for mean dose and DVH dosimetrics, and a p value of ≤ 0.05 indicates statistical significance. Methods with superior performance in all evaluated indices, particularly with no significant difference in D_{NL}^{mean}, D_{Tumors}^{mean}, and D_{Lungs}^{mean} as compared to MC were selected as the best approaches.

Results

Patient and tumor characteristics. The patient characteristics are listed in Table 1. In total, 77 tumors were segmented and analyzed with volume ranging from 12.4 to 1948.2 mL. The NL and lungs volumes ranged from 484.7 to 1900.6 mL and 1958.4 to 3553.9 mL, respectively. The mean density of liver and lung ranges from 1.05 to 1.09 and 0.20 to 0.35 g/cm³, respectively. The TNR and LSF were calculated from Tc-99m-MAA SPECT/CT images for partition model, ranging from 1.3 to 38.9 and 1.5% to 21.2%, respectively.

Mean absorbed dose analysis. The mean absorbed dose difference of partition model and VSV methods compared with MC are reported in Table 2, and the separate results for two datasets are listed in Tables S1 and S2. For D_{NL}^{mean}, LiLuK has the largest deviation of 3.03%, while LiCKLuKD (0.18%) and LiKD (0.23%) have the smallest deviation followed by LiLuKD (0.27%). For D_{Tumors}^{mean}, partition model has the largest deviation (6.36%) among all patients followed by LED and LiLuK. LiLuKD has the smallest deviation followed by LiKD and LiCK-

Patient no.	Microsphere type	LSF (%)	TNR	Tumors vol. (mL)	NL vol (mL)	Liver density (g/cm³)	Lungs vol (mL)	Lung density (g/cm³)
1	Glass	1.5	1.3	20.6	1372.8	1.07 ± 0.01	3591.2	0.27 ± 0.19
2	Glass	8.0	38.9	58.3	1311.1	1.08 ± 0.01	3168.5	0.31 ± 0.21
3	Glass	2.5	15.0	19.26	1787.8	1.07 ± 0.02	1958.4	0.32 ± 0.21
4	Glass	2.1	2.8	71.58	1589.3	1.07 ± 0.01	2701.3	0.29 ± 0.20
5	Glass	2.9	4.2	24.70	1628.6	1.05 ± 0.02	2666.2	0.32 ± 0.21
6	Glass	6.6	3.1	95.94	1276.7	1.07 ± 0.02	3553.9	0.25 ± 0.23
7	Resin	13.7	3.6	1930.0	1033.5	1.07 ± 0.05	3297.3	0.25 ± 0.20
8	Resin	5.8	8.1	183.6	1359.5	1.07 ± 0.06	3144.4	0.31 ± 0.23
9	Resin	2.7	1.7	318.3	999.6	1.07 ± 0.09	2631.9	0.29 ± 0.23
10	Resin	3.2	4.7	1948.2	1483.5	1.08 ± 0.05	2258.3	0.27 ± 0.20
11	Resin	7.3	2.2	857.3	1086.2	1.07 ± 0.07	3022.3	0.23 ± 0.17
12	Resin	2.2	4.2	12.4	1019.4	1.08 ± 0.08	2331.7	0.26 ± 0.18
13	Resin	1.7	2.3	129.5	1187.9	1.08 ± 0.06	2379.9	0.25 ± 0.18
14	Resin	1.6	2.4	285.6	1900.6	1.08 ± 0.07	3791.4	0.22 ± 0.15
15	Resin	17.8	17.3	319.4	700.9	1.10 ± 0.02	3754.4	0.22 ± 0.17
16	Resin	4.8	1.6	228.3	1164.1	1.08 ± 0.02	3774.8	0.20 ± 0.14
17	Glass	4.6	6.3	152.1	1671.7	1.09 ± 0.03	2682.7	0.35 ± 0.17
18	Resin	8.2	3.9	685.0	1040.2	1.09 ± 0.03	2718.6	0.31 ± 0.20
19	Resin	21.2	2.5	899.7	484.7	1.09 ± 0.02	2851.8	0.24 ± 0.17
20	Resin	6.7	1.2	1329.1	1280.3	1.08 ± 0.02	2090.3	0.34 ± 0.14

Table 1. Patient characteristics. *LSF* lung shunt fraction, *TNR* tumor to normal liver ratio, *NL* non-tumoral liver.

Methods	Partition model	LED	LiK	LiLuK	LiKD	LiCK	LiLuKD	LiCKLuKD
D_{NL}^{mean}	1.13 ± 1.42 [0.14, 4.20]	0.97 ± 1.24 [0.01, 3.92]	1.65 ± 0.92 [0.54, 3.90]	3.03 ± 1.40 [0.36, 6.55]	0.23 ± 0.16 [0.01, 0.59]	0.76 ± 0.57 [0.40, 2.74]	0.27 ± 0.16 [0.03, 0.66]	0.18 ± 0.14 [0.02, 0.54]
D_{tumors}^{mean}	2.63 ± 1.65 [0.43, 6.36]	2.59 ± 1.62 [0.40, 6.16]	1.39 ± 0.85 [0.00, 3.17]	2.00 ± 0.92 [0.57, 3.25]	0.58 ± 1.22 [0.02, 5.45]	1.06 ± 1.16 [0.43, 5.52]	0.55 ± 1.21 [0.02, 5.45]	0.64 ± 1.13 [0.02, 4.98]
D_{lungs}^{mean}	8.53 ± 6.52 [0.17, 19.54]	18.48 ± 7.75 [2.70, 34.57]	72.20 ± 4.76 [64.31, 79.05]	18.07 ± 11.22 [0.18, 34.98]	25.02 ± 7.94 [11.70, 42.00]	17.94 ± 6.60 [4.31, 30.62]	9.65 ± 5.59 [0.62, 18.40]	4.86 ± 3.21 [0.79, 15.64]

Table 2. Absolute percent differences of D^{mean} in VOIs using partition model and VSV methods compared with MC. Mean ± std, [min, max].

Methods	Partition model	LED	LiK	LiLuK	LiKD	LiCK	LiLuKD	LiCKLuKD
D_{NL}^{mean}	0.4536	0.2616	**0.0056**	**< 0.0001**	> 0.9999	**0.0040**	0.4536	0.6664
D_{tumors}^{mean}	**< 0.0001**	**< 0.0001**	**< 0.0001**	**< 0.0001**	0.8480	**< 0.0001**	> 0.9999	0.0752
D_{lungs}^{mean}	> 0.9999	**< 0.0001**	**0.008**	> 0.9999	**< 0.0001**	**< 0.0001**	0.3968	> 0.9999
$V_{NL,70Gy}$	N/A	**< 0.0001**	0.2324	**< 0.0001**	0.4284	> 0.9999	**0.0287**	> 0.9999
$V_{tumors,200Gy}$	N/A	**0.0427**	**0.0077**	**< 0.0001**	> 0.9999	> 0.9999	> 0.9999	> 0.9999
$V_{lungs,13Gy}$	N/A	> 0.9999	**< 0.0001**	0.1407	> 0.9999	> 0.9999	> 0.9999	> 0.9999
$V_{lungs,5Gy}$	N/A	**0.0014**	**< 0.0001**	**0.0210**	> 0.9999	> 0.9999	> 0.9999	> 0.9999

Table 3. Statistical analysis results of different VSV and LED dosimetric results as compared to MC. Significant values are in bold.

LuKD. For D_{Lungs}^{mean}, LiCKLuKD has the best agreement with MC result followed by LiLuKD and LiCK. Partition model performs better than the remaining VSV methods and LiK has the poorest performance. Methods with lung kernel or density correction, e.g., LiCKLuKD, LiKD and LiLuK, have improved performance in lungs. Table 3 shows statistical analysis results of different dose conversion methods as compared to MC. The statistical analysis shows that LiK, LiLuK and LiCK have significant differences with MC results in D_{NL}^{mean}. LiKD, LiLuCK and LiCKLuKD have no significant difference with MC results in D_{Tumors}^{mean}. LED, LiK, LiKD and LiCK have significant differences with MC results in D_{Lungs}^{mean}.

3D dosimetrics comparison. Isodose curves and absorbed dose map of a sample patient by MC and VSV methods are shown in Fig. 2. The absorbed dose distributions in liver and tumors are similar for all methods while more a pronounced difference is observed in lungs. Stomach, right kidney and gallbladder also receives radiation from the Y-90 microspheres in liver potentially. The DVH dosimetrics calculated by MC and deviations of VSV generated DVH dosimetrics with MC are reported in Table 4, and the separate results for two datasets are listed in Tables S3 and S4. For $V_{NL,70Gy}$, LiLuK has the largest deviation of 3.03%, while LiKD, LiCK, LiLuKD and LiCKLuKD have better agreement with MC. LED has the largest deviation of 29.29% in $V_{Tumors,200Gy}$, and LiKD, LiCK, LiLuKD and LiCKLuKD have mean deviation < 1.1%. The $V_{Lungs,13Gy}$ and $V_{Lungs,5Gy}$ results are similar. LiK has the largest deviation, while LiLuKD and LiCKLuKD have the smallest deviation. Except for LED, LiLuK and LiCK, other VSV methods have no significant difference with MC in $V_{NL,70Gy}$. LED, LiK, and LiLuK have
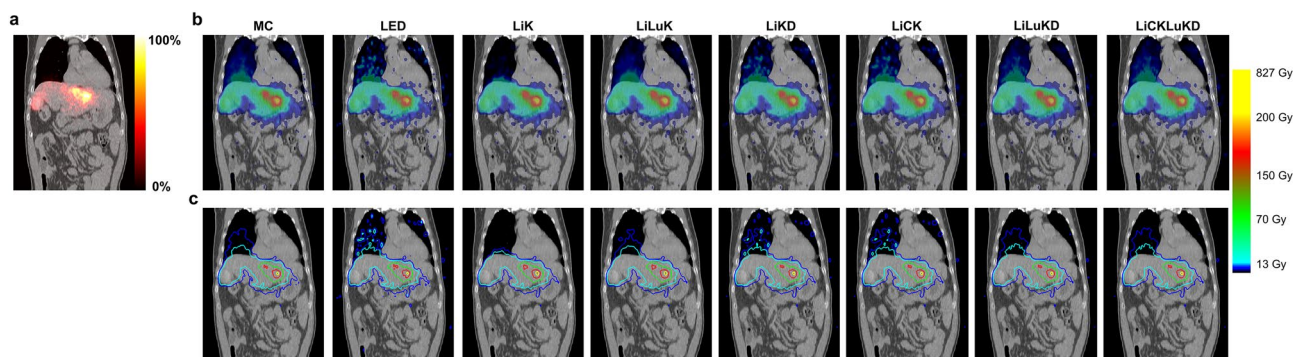
Figure 2. Coronal view of (**a**) the SPECT/CT fusion image, (**b**) the absorbed dose map and (**c**) isodose contour of a sample patient for MC and different VSV methods.

Methods	MC	LED	LiK	LiLuK	LiKD	LiCK	LiLuKD	LiCKLuKD
$V_{NL,70Gy}$	30.09 ± 17.57 [3.43, 58.36]	2.08 ± 1.74 [0.02, 6.01]	1.62 ± 1.32 [0.17, 4.94]	3.03 ± 2.02 [0.27, 8.21]	0.24 ± 0.22 [0.03, 0.99]	0.18 ± 0.22 [0.00, 0.86]	0.30 ± 0.2 [0.00, 0.99]	0.19 ± 0.15 [0.00, 0.51]
$V_{tumors,200Gy}$	43.86 ± 33.89 [0.00, 92.85]	1.60 ± 6.86 [0.00, 29.29]	3.74 ± 5.52 [0.00, 23.91]	4.10 ± 5.48 [0.00, 23.91]	0.83 ± 1.36 [0.00, 5.88]	0.51 ± 0.62 [0.00, 2.02]	0.79 ± 1.36 [0.00, 5.88]	0.42 ± 0.61 [0.00, 2.26]
$V_{lungs,13Gy}$	8.90 ± 8.08 [0.55, 39.61]	13.31 ± 32.24 [2.30, 111.63]	75.25 ± 8.46 [61.22, 96.19]	21.10 ± 19.08 [0.45, 70.21]	24.88 ± 29.45 [0.27, 111.61]	24.24 ± 27.39 [1.34, 106.76]	13.74 ± 19.59 [0.08, 89.19]	12.82 ± 18.88 [0.73, 86.61]
$V_{lungs,5Gy}$	23.09 ± 20.41 [5.86, 81.44]	17.30 ± 9.66 [0.45, 35.99]	67.93 ± 11.11 [55.52, 95.78]	14.30 ± 10.27 [1.95, 35.99]	11.95 ± 8.33 [0.53, 28.15]	11.07 ± 7.80 [0.11, 27.81]	4.76 ± 4.90 [0.38, 16.15]	5.88 ± 4.78 [0.09, 17.10]

Table 4. Absolute percent differences of DVH dosimetrics using VSV methods compared with MC and the dosimetrics calculated by MC. Mean ± std, [min, max].
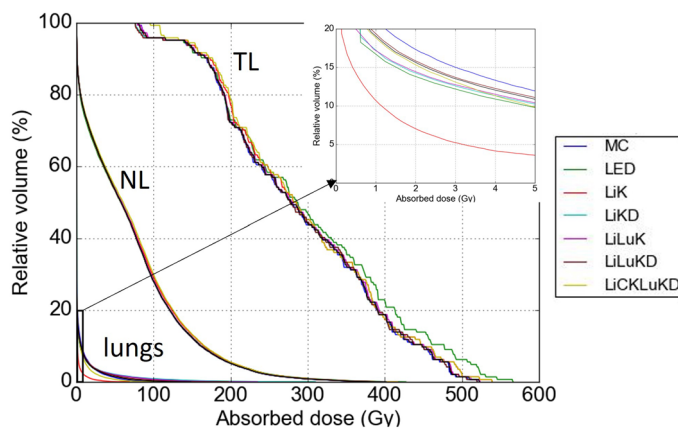
Figure 3. Cumulative DVH for NL, tumors, lungs and magnified image of lungs by MC and VSV methods for another sample patient.

significant differences with MC in $V_{Tumors,200Gy}$. For $V_{Lungs,13Gy}$, only LiK has significant differences with MC, while for $V_{Lungs,5Gy}$, LED, LiK and LiLuK have significant differences with MC.

The cumulative DVH curves of another sample patient for NL, tumors and lungs are shown in Fig. 3. The volume fraction for absorbed dose > 70 Gy in NL takes up ~ 50%. All VSV methods are close to MC in NL. For tumors, LED overestimates the volume fraction in the high absorbed dose region, i.e., ~ 230 to 520 Gy. For lungs, the volume fraction > 5 Gy is about 13% for this patient. LiK has substantially underestimated the volume fraction. As expected, tumors have higher absorbed dose as compared to NL, while lungs have the lowest absorbed dose.

The MAE of differential DVH is reported in Table 5. LiLuK, LED and LiK have the maximum MAE in NL, tumors and lungs, respectively. LiKD, LiCK and LiCKLuKD have lower MAE in NL and tumors. The MAE of LiLuKD is the lowest in lungs followed by LiCKLuKD. The execution time of all VSV methods takes up within 10 s using fast Fourier transform.

MIA comparison. Figure 4 shows the Bland–Altman plots of MIA results between MC and other methods. The restriction of lung absorbed dose was not applied for MIA calculation as D_{Lungs}^{mean} of all patients is well < 30 Gy. The MIA calculated by MC are regarded as the baseline, ranging from 1.67 to 15.51 GBq. Partition model and VSV methods except for LiCK have a deviation of < 5% in MIA calculation compared with MC.

VSV methods	LED	LiK	LiLuK	LiKD	LiCK	LiLuKD	LiCKLuKD
NL	28.92	20.05	35.74	4.10	4.59	8.37	2.98
Tumors	202.16	98.53	133.07	31.35	30.79	47.25	27.22
Lungs	36.51	77.14	22.12	38.02	38.02	8.37	11.12

Table 5. MAE of differential DVH by VSV methods in different VOIs compared with MC.
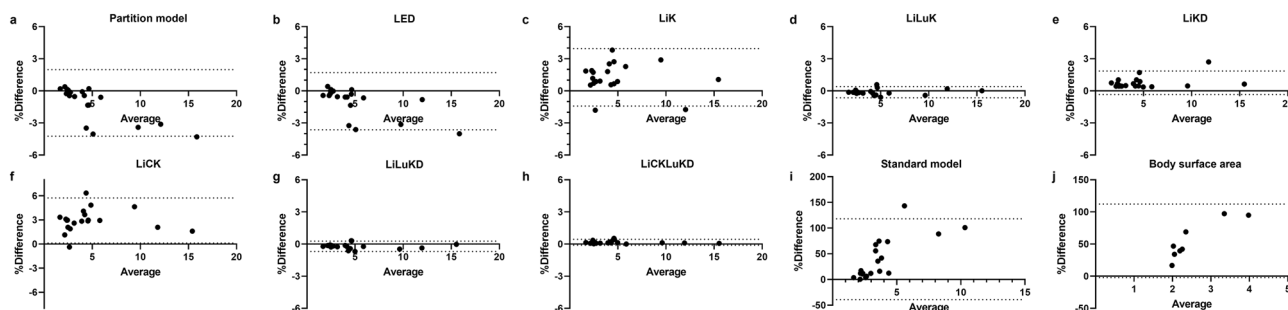
Figure 4. Bland–Altman plots with 95% confidence interval (CI) of MIA differences (%) between MC and other methods. The dashed lines represent 95% CI of mean differences.

Discussion

The MIA of Y-90 RE is usually based on conventional 2D models such as partition model and body surface area method currently in the clinic. However, these methods do not consider the heterogeneity of microspheres distribution. Some groups also proposed 3D treatment planning method for Y-90 RE. Morán et al.[21] compared different dose conversion methods, standard partition model, partition model considering multiple tumors, LED and LiK. Dieudonné et al.[19] proposed a 3D dose conversion method for treatment planning by LiK. However, both of them did not consider potential variations in lung absorbed dose estimation and did not compare their results with MC simulations. Petitguillaume et al.[20] used the DVH dosimetrics by MC simulations for Y-90 RE treatment planning but not for VSV. In this study we show that VSV is an alternative to partition model and MC in MIA calculation, and is feasible to provide accurate and complete DVH dosimetrics for Y-90 RE treatment planning in real time.

VSV methods could provide slightly better estimation on D_{Tumors}^{mean} than partition model and the performance of VSV methods are improved by applying density corrections. LiK has similar results with partition model on D_{NL}^{mean} and D_{Tumors}^{mean} consistent with Dieudonné et al.[19]. LED does not consider the cross-voxel radiation, with a deviation of 6.16% for tumors. Partition model, LED and LiK have larger difference of D_{Tumors}^{mean} than D_{NL}^{mean}, consistent with the results of Morán et al.[21]. Hashikin et al.[34] shows more pronounced absorbed dose difference of tumors and NL in partition model as compared to MC in phantom simulations. This difference in real patients may be less obvious due to the tumor VOIs may be generally larger on SPECT to compensate for the partial volume effect, thus alleviating the errors of partition model in not modeling the cross-radiation effect. Tumors and NL possess similar density thus their dosimetric accuracy is expected to be similar. Our results show that the error is slightly higher for tumors, which could be attributed to the more pronounced partial volume effect for tumors. The limit of D_{Tumors} are not considered in IA calculation currently, as functions of the critical organs are of primarily concern to minimize toxicity. However, tumor dosimetry would be of interest as an indicator for tumor response[35–37].

The lung absorbed dose errors are much larger than tumors and NL in general, as activity from liver has potential contributions and cannot be adequately modeled from some evaluated methods. The lung tissue is also quite heterogeneous, with densities range from 0.00126 g/cm³ (air) to 1.04 g/cm³ (soft tissue), posing significant problems for methods without density corrections. LiK has the largest deviation in D_{Lungs}^{mean} due to the large difference of density between liver and lung medium. The assumed densities of liver and lungs are close to the mean liver and lungs density of different patients in this study, verifying the accuracies of VSV kernels generated in the assumed liver and lung media. The usage of lung kernel, e.g., LiLuK, could improve D_{Lungs}^{mean} estimation, consistent with results of Mikell et al.[9]. LiCK has higher errors in D_{NL}^{mean} and D_{Tumors}^{mean} than LiKD, and less errors in D_{Lungs}^{mean}, consistent with results from Götz et al.[17]. Thus, a combination of center voxel scaling and density correction could further improve the performance of LiLuK and LiLuKD, i.e., LiCKLuKD as proposed in this study, which has better performance in lungs.

The DVH dosimetrics results are similar to mean absorbed dose. The VSV methods with corrections, i.e., LiKD, LiLuKD and LiCKLuKD, could achieve < 5.88% deviation of $V_{NL, 70 Gy}$ and $V_{Tumors, 200 Gy}$. In addition, both LiLuKD and LiCKLuKD have < 14% mean deviation for $V_{Lungs, 13 Gy}$ and < 5% mean deviation for $V_{Lungs, 5 Gy}$, respectively, outperforming other VSV methods. However, D_{Lungs}^{mean} was more relevant than DVH of lungs in predicting clinically significant radiation pneumonitis in external beam radiotherapy[38]. LSF is also considered to be correlated with radiation pneumonitis in Y-90 RE[39]. Thus, the DVH of the lungs may be not a critical factor for determining MIA in Y-90 RE. The performances of VSV methods on MAE are consistent with results of the DVH dosimetrics. LiKD, LiCK, LiLuKD and LiCKLuKD have smaller deviation on NL and tumors. LiCKLuKD has the smallest deviation of DVH of lungs.

The calculation of MIA depends on D_{NL}^{mean} and D_{Lungs}^{mean}, though the prescription is usually bounded by D_{NL}^{mean} instead of D_{Lungs}^{mean} as the later dose limit is usually not reached. However, patients are commonly excluded for treatment if their LSF > 20%. This criteria may not be translated to D_{Lungs}^{mean} > 30 Gy as shown in this study (Patient 19, LSF = 21.2%, D_{Lungs}^{mean} = 16.07 Gy by MC), while D_{Lungs}^{mean} of Patient 2 is > 20 Gy with LSF = 8.0%. Thus, LSF > 20% may not be a good criteria for excluding patients from Y-90 RE, as indicated by the latest user manual[6]. The MIA difference between VSV and partition model is negligible, consistent with Dieudonné et al.[19], while Petitguillaume et al.[20] observed a bigger difference. The discrepancy could be attributed to the difference in activity calibration method. They also showed that the MIA could be further increased based on DVH dosimetrics instead of mean absorbed dose, yet the clinical application of the DVH dosimetrics still needs to be further studied. Notably, the partition model has comparable performance with MC in MIA and other VSV methods in MIA. Thus, its clinical effectiveness is justified especially considering its relatively simple implementation. However, VSV methods can be used to replace partition model for MIA calculation in the clinics, with the advantage of providing further 3D dosimetric information. Considering the real-time execution, relatively small dosimetrics errors, and with no significant difference as compared with MC in mean dose of NL, tumors and lungs, LiLuKD and LiCKLuKD are recommended for absorbed dose conversion.

We implemented the density correction (Eq. 5) differently as compared to ref 14, to be consistent with the center voxel scaling (Eq. 6) implementation. Both should yield the same results as the convolution is a linear operator. The accuracy of VSV methods using tissue specific kernels depends on the segmentations of liver and lungs, which are expected to be less subjected to errors based on CT data. However, mismatches between emission imaging data and the corresponding CT also impact VSV-based dosimetry, and are evaluated in our previous studies[40–42]. Registrations between CT and emission imaging data will ease this concern[43]. To the best of our knowledge, this is the first study to systematically analyze different VSV methods for Y-90 RE based on Tc-99m SPECT/CT. One limitation of our study is that the distributions of pre-treatment Tc-99m SPECT images and post-treatment Y-90 PET or SPECT images may not be exactly the same and could be affected by many

factors, e.g., catheter positioning, particle size, liver and lungs volume[44]. The performance of VSV methods on post-therapy voxel level dosimetry, i.e., Y-90 microsphere SPECT and Y-90 microsphere PET, is investigated in another study from our group, where LiLuKD and LiCKLuKD still demonstrate superior performance as compared to other methods[22].

Conclusion

Seven VSV methods were evaluated for the 3D absorbed dose conversion in 20 patients with pre-treatment Tc-99m-MAA SPECT/CT images for Y-90 RE, along with partition model and MC. VSV methods with effective correction and tissue-specific kernel, i.e., LiLuKD and our proposed LiCKLuKD, could provide MIA consistent with partition model, and additional precise DVH dosimetrics for potential improved treatment planning considering radiobiological effects.

Data availability

The first datasets analyzed during the current study are available in the University of Michigan—Deep Blue Data repository, [https://doi.org/10.7302/pf4m-vn04]. The second data analyzed during the current study are not publicly available due to ethical requirements for hospitals but are available from the corresponding author on reasonable request.

References

1. Sangro, B. *et al.* Radioembolization using 90Y-resin microspheres for patients with advanced hepatocellular carcinoma. *Int. J. Radiat. Oncol*. Biol*. Phys.* **66**, 792–800 (2006).
2. Gabr, A. *et al.* Correlation of Y90-absorbed radiation dose to pathological necrosis in hepatocellular carcinoma: Confirmatory multicenter analysis in 45 explants. *Eur. J. Nucl. Med. Mol. Imaging* **48**, 580–583 (2021).
3. Walrand, S., Hesse, M., Chiesa, C., Lhommel, R. & Jamar, F. The low hepatic toxicity per Gray of 90Y glass microspheres is linked to their transport in the arterial tree favoring a nonuniform trapping as observed in posttherapy PET imaging. *J. Nucl. Med.* **55**, 135–140 (2014).
4. Salem, R. *et al.* Incidence of radiation pneumonitis after hepatic intra-arterial radiotherapy with yttrium-90 microspheres assuming uniform lung distribution. *Am. J. Clin. Oncol.* **31**, 431–438 (2008).
5. Li, T. *et al.* Quantitative imaging for targeted radionuclide therapy dosimetry-technical review. *Theranostics* **7**, 4551 (2017).
6. Sirtex, M. *Sirtex Package Insert*. https://www.sirtex.com/media/ka0f3aaz/ifu-006-row-sir-spheres-microspheres-ifu-for-row.pdf (2022).
7. Chiesa, C. *et al.* EANM dosimetry committee series on standard operational procedures: A unified methodology for 99mTc-MAA pre-and 90Y peri-therapy dosimetry in liver radioembolization with 90Y microspheres. *EJNMMI Phys.* **8**, 1–44 (2021).
8. Biocompatibles, U. K. *Therasphere (TM) package insert*. https://www.bostonscientific.com/content/dam/elabeling/pi/OTT-00221_Rev1_TheraSphere_en_s.pdf (2014).
9. Mikell, J. K. *et al.* Selective internal radiation therapy with yttrium-90 glass microspheres: Biases and uncertainties in absorbed dose calculations between clinical dosimetry models. *Int. J. Radiat. Oncol*. Biol*. Phys.* **96**, 888–896 (2016).
10. Ho, S. *et al.* Partition model for estimating radiation doses from yttrium-90 microspheres in treating hepatic tumours. *Eur. J. Nucl. Med.* **23**, 947–952 (1996).
11. Veenstra, E. B. *et al.* Post-treatment three-dimensional voxel-based dosimetry after Yttrium-90 resin microsphere radioembolization in HCC. *EJNMMI Res.* **12**, 1–9 (2022).
12. Willowson, K. P., Schembri, G. P., Bernard, E. J., Chan, D. L. & Bailey, D. L. Quantifying the effects of absorbed dose from radioembolisation on healthy liver function with [99mTc] Tcmebrofenin. *Eur. J. Nucl. Med. Mol. Imaging* **47**, 838–848 (2020).
13. Bolch, W. E. *et al.* MIRD pamphlet no. 17: The dosimetry of nonuniform activity distributions—radionuclide S values at the voxel level. *J. Nucl. Med.* **40**, 11–36 (1999).
14. Mok, G. S. & Dewaraja, Y. K. Recent advances in voxel-based targeted radionuclide therapy dosimetry. *Quant. Imaging Med. Surg.* **11**, 483 (2021).
15. Dieudonné, A. *et al.* Study of the impact of tissue density heterogeneities on 3-dimensional abdominal dosimetry: Comparison between dose kernel convolution and direct Monte Carlo methods. *J. Nucl. Med.* **54**, 236–243 (2013).
16. Lee, M. S. *et al.* Whole-body voxel-based personalized dosimetry: The multiple voxel S-value approach for heterogeneous media with nonuniform activity distributions. *J. Nucl. Med.* **59**, 1133–1139 (2018).
17. Götz, T. *et al.* A comparison of methods for adapting dose-voxel-kernels to tissue inhomogeneities. *Phys. Med. Biol.* **64**, 245011 (2019).
18. Mikell, J. K., Mahvash, A., Siman, W., Mourtada, F. & Kappadath, S. C. Comparing voxel-based absorbed dosimetry methods in tumors, liver, lung, and at the liver-lung interface for 90Y microsphere selective internal radiation therapy. *EJNMMI Phys.* **2**, 1–14 (2015).
19. Dieudonné, A. *et al.* Clinical feasibility of fast 3-dimensional dosimetry of the liver for treatment planning of hepatocellular carcinoma with 90Y-microspheres. *J. Nucl. Med.* **52**, 1930–1937 (2011).
20. Petitguillaume, A. *et al.* Three-dimensional personalized Monte Carlo dosimetry in 90Y resin microspheres therapy of hepatic metastases: Nontumoral liver and lungs radiation protection considerations and treatment planning optimization. *J. Nucl. Med.* **55**, 405–413 (2014).
21. Morán, V. *et al.* Impact of the dosimetry approach on the resulting 90Y radioembolization planned absorbed doses based on 99mTc–MAA SPECT-CT: Is there agreement between dosimetry methods?. *EJNMMI Phys.* **7**, 1–22 (2020).
22. Chen, G., Lu, Z., Chen, Y. & Mok, G. S. Voxel-S-value methods adapted to heterogeneous media for quantitative Y-90 microsphere radioembolization dosimetry. *Z. Med. Phys.* https://doi.org/10.1016/j.zemedi.2022.11.003 (2022).
23. Van, B. J., Dewaraja, Y. K. Y-90 PET/CT & SPECT/CT and corresponding contours dataset 31JULY2020. *University of Michigan - Deep Blue Data* (2020).
24. Van, B. J., Dewaraja, Y. K., Sangogo, M. L. & Mikell, J. K. Y-90 SIRT: Evaluation of TCP variation across dosimetric models. *EJNMMI Phys.* **8**, 1–14 (2021).
25. Klein, S., Staring, M., Murphy, K., Viergever, M. A. & Pluim, J. P. Elastix: A toolbox for intensity-based medical image registration. *IEEE Trans. Med. Imaging* **29**, 196–205 (2009).
26. Schneider, W., Bortfeld, T. & Schlegel, W. Correlation between CT numbers and tissue parameters needed for Monte Carlo simulations of clinical dose distributions. *Phys. Med. Biol.* **45**, 459 (2000).

27. Kim, S. P., Juneau, D., Cohalan, C. & Enger, S. A. Standardizing SPECT/CT dosimetry following radioembolization with yttrium-90 microspheres. *EJNMMI Phys.* **8**, 1–19 (2021).
28. Papadimitroulas, P., Loudos, G., Nikiforidis, G. C. & Kagadis, G. C. A dose point kernel database using GATE Monte Carlo simulation toolkit for nuclear medicine applications: Comparison with other Monte Carlo codes. *Med. Phys.* **39**, 5238–5247 (2012).
29. Brosch-Lenz, J. *et al.* Influence of dosimetry method on bone lesion absorbed dose estimates in PSMA therapy: Application to mCRPC patients receiving Lu-177-PSMA-I&T. *EJNMMI Phys.* **8**, 1–17 (2021).
30. Sirtex, M. *Sirtex Package Insert*. http://www.radmed.com.tr/usr_img/sir_spheres/pdf/package_insert_sirtex.pdf (2005).
31. Kao, Y. H., Tan, E. H., Ng, C. E. & Goh, S. W. Clinical implications of the body surface area method versus partition model dosimetry for yttrium-90 radioembolization using resin microspheres: A technical review. *Ann. Nucl. Med.* **25**, 455–461 (2011).
32. Mayo, C. S. *et al.* Hybrid IMRT for treatment of cancers of the lung and esophagus. *Int. J. Radiat. Oncol*. Biol*. Phys.* **71**, 1408–1418 (2008).
33. Ao, E. C., Wu, N. Y., Wang, S. J., Song, N. & Mok, G. S. Improved dosimetry for targeted radionuclide therapy using nonrigid registration on sequential SPECT images. *Med. Phys.* **42**, 1060–1070 (2015).
34. Hashikin, N. A. A. *et al.* Systematic investigation on the validity of partition model dosimetry for 90Y radioembolization using Monte Carlo simulation. *Phys. Med. Biol.* **62**, 7342 (2017).
35. Chansanti, O. *et al.* Tumor dose response in yttrium-90 resin microsphere embolization for neuroendocrine liver metastases: A tumor-specific analysis with dose estimation using SPECT-CT. *J. Vasc. Interv. Radiol.* **28**, 1528–1535 (2017).
36. Kappadath, S. C. *et al.* Hepatocellular carcinoma tumor dose response after 90Y-radioembolization with glass microspheres using 90Y-SPECT/CT-based voxel dosimetry. *Int. J. Radiat. Oncol*. Biol*. Phys.* **102**, 451–461 (2018).
37. Alsultan, A. A. *et al.* Dose-response and dose-toxicity relationships for yttrium-90 glass radioembolization in patients with colorectal cancer liver metastases. *J. Nucl. Med.* https://doi.org/10.2967/jnumed.120.255745 (2021).
38. Wang, W. *et al.* Effect of normal lung definition on lung dosimetry and lung toxicity prediction in radiation therapy treatment planning. *Int. J. Radiat. Oncol*. Biol*. Phys.* **86**, 956–963 (2013).
39. Arroyo-Hernández, M. *et al.* Radiation-induced lung injury: Current evidence. *BMC Pulm. Med.* **21**, 1–12 (2021).
40. Lu, Z., Chen, G., Lin, K. H., Wu, T. H. & Mok, G. S. Evaluation of different CT maps for attenuation correction and segmentation in static 99mTc-MAA SPECT/CT for 90Y radioembolization treatment planning: A simulation study. *Med. Phys.* **48**, 3842–3851 (2021).
41. Lyu, Y., Chen, G., Lu, Z., Chen, Y. & Mok, G. S. The effects of mismatch between SPECT and CT images on quantitative activity estimation—a simulation study. *Z. Med. Phys.* https://doi.org/10.1016/j.zemedi.2022.03.004 (2022).
42. Lu, Z., Chen, G., Lyu, Y., Chen, Y. & Mok, G. S. Respiratory impacts on static and respiratory gated 99mTc-MAA SPECT/CT for liver radioembolization—a simulation study. *Med. Phys.* **49**, 5330–5339 (2022).
43. Lu, Z. *et al.* SPECT and CT misregistration reduction in [99mTc]Tc-MAA SPECT/CT for precision liver radioembolization treatment planning. *Eur. J. Nucl. Med. Mol. Imaging*. https://doi.org/10.1007/s00259-023-06149-9 (2023).
44. Knešaurek, K., Tuli, A., Pasik, S. D., Heiba, S. & Kostakoglu, L. Quantitative comparison of pre-therapy 99mTc-macroaggregated albumin SPECT/CT and post-therapy PET/MR studies of patients who have received intra-arterial radioembolization therapy with 90Y microspheres. *Eur. J. Radiol.* **109**, 57–61 (2018).

Acknowledgements

Author contributions

G.C. designed and executed the experiment and drafted most parts of the manuscript. Z.L. and H.J. provide some instructions on partition model and image segmentation. K.L. provides image dataset and instructions on partition model. G.M. is responsible for the conceptualization and supervision of the project, and drafted the manuscript.

Competing interests

The authors declare no competing interests.

Additional information

Supplementary Information The online version contains supplementary material available at https://doi.org/10.1038/s41598-023-30824-4.

Correspondence and requests for materials should be addressed to G.S.P.M.

Reprints and permissions information is available at www.nature.com/reprints.

Publisher's note Springer Nature remains neutral with regard to jurisdictional claims in published maps and institutional affiliations.